



Synthesis of superparamagnetic iron oxide nanoparticles coated with polyethylene glycol as potential drug carriers for cancer treatment

D. LLamosa Pérez · I. Puentes ·
G. A. Murillo Romero · I. M. Saavedra Gaona ·
C. A. Parra Vargas · R. J. Rincón

Received: 5 July 2023 / Accepted: 15 November 2023 / Published online: 20 December 2023
© The Author(s) 2023

Abstract Current cancer treatments are not selective in delivering drugs to cancer cells, affecting healthy tissues and especially rapidly dividing cells. This work describes the development of superparamagnetic nanoparticles for drug delivery through green synthesis, mediated by *Musa paradisiaca* peel extract as a stabilizing and reducing agent. The nanoparticles' structural, morphological, magnetic and chemical properties were evaluated. The XRDs showed a cubic crystal structure with the space group of $Fd\bar{3}m$ (No. 227), typical of magnetite. Through SEM and TEM, it was determined that the mean size of the nanoparticles was 11.61 nm. FTIR and EDS confirmed the successful synthesis of Fe_3O_4 nuclei, covered with polyethylene glycol and loaded with doxorubicin. The magnetic properties of the nanocomposites obtained were measured using VSM, evidencing a superparamagnetic behaviour with a $M_s = 72.75$ emu/g. Finally, MTT assays on the HeLa tumour line showed a 45.5% decrease in cell viability.

The determined properties allow the application of the nanocomposite produced as a potential candidate for cancer treatment.

Keywords Nanoparticles · Superparamagnetic iron oxide · Functionalization · Ultrasound · Polyethylene glycol · Doxorubicin · Drug delivery

Introduction

Cancer is one of the most widely attended diseases today as it is among the leading causes of death worldwide, leaving almost 10 million dead in 2020 [1]; surgery, immunotherapy, radiation therapy, targeted therapies, hormone therapies, stem cell transplants and chemotherapy are not selective, causing toxicity and side effects to the body [2]. That is why implementing new treatments are sought, improving existing ones by increasing their specificity and even developing personalized therapies.

Nanotechnology is a field recently explored in medicine for its particularity in using different materials at the nanometric scale (a nanometre is one billionth of a meter, 1×10^{-9} m) [3]. In this field, nanomedicine explores the relationship between biological systems and nanometric materials [4]. In nanomedicine, nanometric materials will enable the construction, repair, control and monitoring of human biological systems at the molecular scale, using nanodevices and nanostructures that can benefit the research

D. L. Pérez (✉) · I. Puentes · G. A. M. Romero ·
R. J. Rincón

Grupo de Investigación Fundamental y Aplicada en
Materiales, Facultad de Ciencias, Universidad Antonio
Nariño, Sede Circunvalar, Carrera 1a Este #47A15,
CP 110231 Bogotá, D.C., Colombia
e-mail: dllamosa@uan.edu.co

I. M. S. Gaona · C. A. P. Vargas
Grupo Física de Materiales, Escuela de Física, Universidad
Pedagógica y Tecnológica de Colombia, Avenida Central
del Norte, 39-115, 150003 Tunja, Boyacá, Colombia

and practice of medicine [5]. Nanoparticles (NPs), ranging in size from 1 to 100 nm, have outstanding properties such as surface adaptability, improved solubility and multi-functionality. These novel characteristics that differ markedly from the properties exhibited by materials at the micro and macroscopic scale allow the passage to new research, having the ability to interact with complex biological functions, operating at the same scale of biomolecules [6], so its use in medicine is of interest for bioavailability processes of poorly soluble drugs, drug delivery vehicles to develop controlled release to specific sites and vaccine aids and diagnostics [7]. Several nanoparticle (NPs) types have been proposed for therapeutic applications, including micelles, dendrimers, polymeric, metallic, silica and cell membrane-coated nanoparticles [8].

Among the NPs studied, iron oxide NPs smaller than 150 nm are known as SPION (super para-magnetic iron-oxide nanoparticles) [9]. SPIONs are characterized by superparamagnetic behaviour. In other words, SPIONs manifest their magnetic properties only when subjected to an external magnetic field. Thanks to their superparamagnetic properties and biocompatibility with the organism [10], SPIONs could be controlled and guided to a specific tissue or organ by an external magnetic field [11]. These SPION characteristics generate a wide range of applications in medicine [12]. The surface of these NPs can be modified, coating the magnetic core with polymers to obtain colloidal stability in aqueous media. SPION can be coupled with several molecules, such as a drug, with these surface modifications. By performing a surface functionalization, the nanoparticles are prevented from being recognized by the body's macrophages. The polymers used must provide characteristics such as colloidal stability in the blood system, being hydrophilic, avoiding opsonization (interaction with specific proteins that mark nanoparticles for their subsequent phagocytosis) as they are non-ionic polymers and having a considerable molecular weight to promote spherical protection [13]. One of the polymers that meet these characteristics is polyethylene glycol (PEG), which has a molecular weight of < 20 kDa [14]. It has been found that coating nanoparticles with PEG alters cell uptake and increases blood circulation time, improves stability, increases solubility and decreases renal proteolysis and excretion. PEGylation creates a hydrophilic layer around

the nanoparticle that blocks electrostatic and hydrophobic interactions that help opsonins bind to particle surfaces [15].

The synthesis of NPs by conventional methodologies employs chemical agents that can generate environmental pollution. To minimize these drawbacks, green synthesis emerges as an alternative to produce materials at the nanometer scale. Green synthesis is based on reducing metals by natural species with antioxidant power, using bacteria, fungi and plant extracts or parts thereof. Some plants contain metabolites with reducing properties, such as phenolic compounds, mainly gallic acid, benzoic acid and caffeic acid, giving them antioxidant properties. The use of these extracts induces the formation of nucleation centres, which sequester metal ions, leading to the formation of nanoparticles. Additionally, with these extracts, it is possible to stabilize the size of the NPs and prevent them from being added [16]. Agro-industrial residues such as banana peel (*Musa paradisiaca*) can be used to obtain extracts. This has a large percentage of phytochemicals, primarily antioxidants, such as gallic catechin [17], found in a more significant proportion. Other antioxidants are phenolic compounds, anthocyanins, delphinidin, cyanidin and catecholamines [18]. These phytochemicals act as stabilizing agents by controlling the size and morphology of NPs by preventing their aggregation [19, 20].

Numerous investigations have focused on searching for methods of synthesis of NPs and extraction of bioactive substances that are fast, eco-friendly and economical. The sonochemical method is most suitable for synthesizing NPs that meet the above parameters [21–23]. Sonication allows superior yields in little time; it has been reported that among nanoparticle synthesis methods, this method presents a green, economically viable and ecologically sustainable approach to the synthesis of NPs at the industrial level [22, 24]. This method is based on the high energy of ultrasonic waves through a fluid, creating high- and low-pressure cycles and giving rise to cavitation [25]. The microbubbles' formation, growth and implosive collapse generated effects such as erosion, particle decomposition, sonoporation and cell disruption [26].

Due to the above problems and challenges identified, the present research proposes synthesizing superparamagnetic iron oxide nanoparticles using *Musa paradisiaca* extract, coating them with

polyethylene glycol (SPION@PEG), as a viable system for the transport and administration of an anti-cancer drug.

Materials and methods

Materials

The reagents used for the synthesis of SPION coated with PEG were iron(II) chloride tetrahydrate ($\text{FeCl}_2 \cdot 4\text{H}_2\text{O}$, Merck), iron(III) chloride hexahydrate ($\text{FeCl}_3 \cdot 6\text{H}_2\text{O}$, Merck), 25% ammonium hydroxide (NH_4OH , CMLAB), polyethylene glycol with a molecular weight of 1000 g/mol (PEG, Aldrich), sodium dodecyl sulfate (SDS, PanReac AppliChem) and *Musa paradisiaca* peel extract. Type I ultrapure water was used throughout the process. The anticancer drug tested was doxorubicin hydrochloride (DOX, Blau).

MTT (3-(3,4-dimethylthiazol-2-yl)-2,5-diphenyltetrazolium bromide) assays were performed to evaluate cytotoxicity. The following reagents were required: DMEM (Gibco Dulbecco's modified Eagle medium, BioWhittaker), foetal bovine serum (Biowest) for cell cultures, phosphate-buffered saline (PBS, BioWhittaker), trypsin (Veisene), MTT (Trevigen) and DMSO (dimethyl sulfoxide, BioBasic). The cell culture corresponds to the HeLa human cervical adenocarcinoma cell line.

Obtaining the extract of *Musa paradisiaca*

The ultrasound-assisted extraction technique (Fig. 1) obtained the *Musa paradisiaca* extract. A total of 50.0 g of *Musa paradisiaca* peel, previously washed with water and an approximate particle size of 1 cm^2 , was massed. Later, they were added to 100.0 mL of water. It was irradiated with ultrasound for 7 min (UP400St, Hielscher), using a titanium probe of

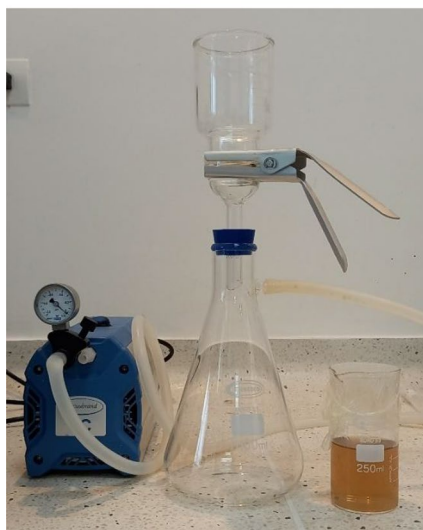
Fig. 1 Ultrasound-assisted extraction: (a) ultrasound (UP400St, Hielscher), (b) mechanical agitation (Hei-Torque 200)



Musa Paradisiaca



Fragments approximately 1 cm^2



Centrifuge and vacuum filtering



Ultrasound with mechanical agitation

22 mm in diameter, at a frequency of 45 kHz, with an amplitude of 60 μm , at a temperature of 39 °C and a specific energy supplied of 124.236 J/mL. Mechanical agitation (Hei-Torque 200) kept the reaction medium homogeneous at 400 rpm. The mixture produced was filtered and centrifuged at 4500 rpm for 20 min (Thermo Scientific, SL 8R). Finally, the supernatant was vacuum-filtered and stored for SPION synthesis.

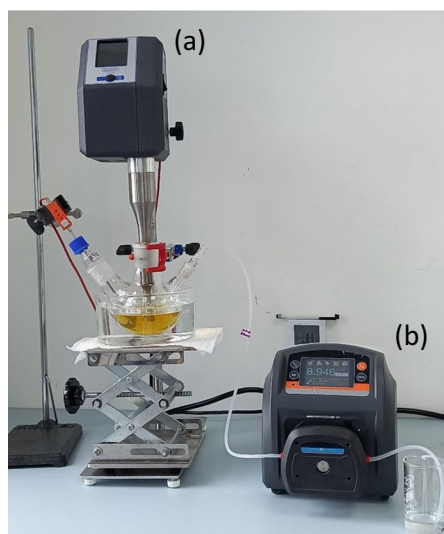
Synthesis of SPIONs coated with PEG (SPION@PEG)

SPIONs were synthesized by coprecipitation of iron chlorides, assisting with ultrasonic cavitation (UP400St, Hielscher); see Fig. 2. Briefly, a precursor solution was prepared using iron chlorides (II and III) in a molar ratio 1:2, respectively, dissolving 516.67 mg of $\text{FeCl}_2 \cdot 4\text{H}_2\text{O}$ and 1405.07 mg of $\text{FeCl}_3 \cdot 6\text{H}_2\text{O}$ in 100.0 mL of water. The iron oxide was coprecipitated by adding 50.0 mL of an NH_4OH solution drop by drop until it reached a pH of 11.25. At the end of this first stage, 50.0 mL of *Musa Paradisiaca* extract and NH_4OH (4 mL) was added drop by drop. The drip speed at each stage was 8.9 mL/min. This speed was controlled by a peristaltic pump (BT101F). During the dripping of the solutions, it was irradiated with ultrasounds using a titanium probe of 22 mm in diameter at a frequency

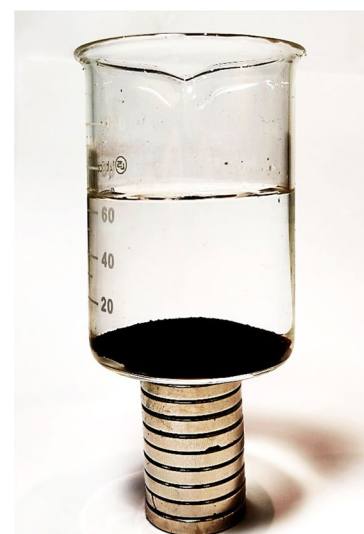
of 45 kHz, with an amplitude of 60 μm and a specific energy supply of 329.47 J/mL. The colloidal dispersion of the SPION produced was magnetically assisted decanted (using a permanent neodymium magnet). The supernatant was discarded, and the precipitate was washed with water type I twice. The SPIONs were divided into two portions, one to advance the characterization of these uncoated, drying them in an oven (Thermo Scientific) at 90 °C for 24 h, and the other fraction was used to be coated with PEG and obtain the nanocomposite SPION@PEG.

Two solutions were prepared for coating the SPIONs (Fig. 3). In the first one, 540 mg of SDS was dissolved in 25.0 mL of water to promote the dispersion of the nanoparticles; in the second solution, 66.5 mg of PEG was dissolved in 25.0 mL of water. Both solutions were homogenized in an ultrasonic bath (Elmasonic S30H) for 1 min. A portion of the precipitate obtained from the SPION was re-suspended in 100.0 mL of water using the ultrasound bath (Elmasonic S30H) for 1 min. Subsequently, the drop-by-drop solutions were added separately at an 8.9 mL/min rate, controlled through the peristaltic pump (BT101F). The SDS solution was dripped first, followed by the PEG solution after incorporating both solutions and was sonicated for 5 min to ensure the homogenization of the NPs. The particles thus

Fig. 2 Ultrasound-assisted SPION biosynthesis. (a) Ultrasound (UP400St, Hielscher), (b) peristaltic pump (BT101F)



Iron chloride coprecipitación,
asisted by ultrasonidos



Magnetically assisted
settling separation

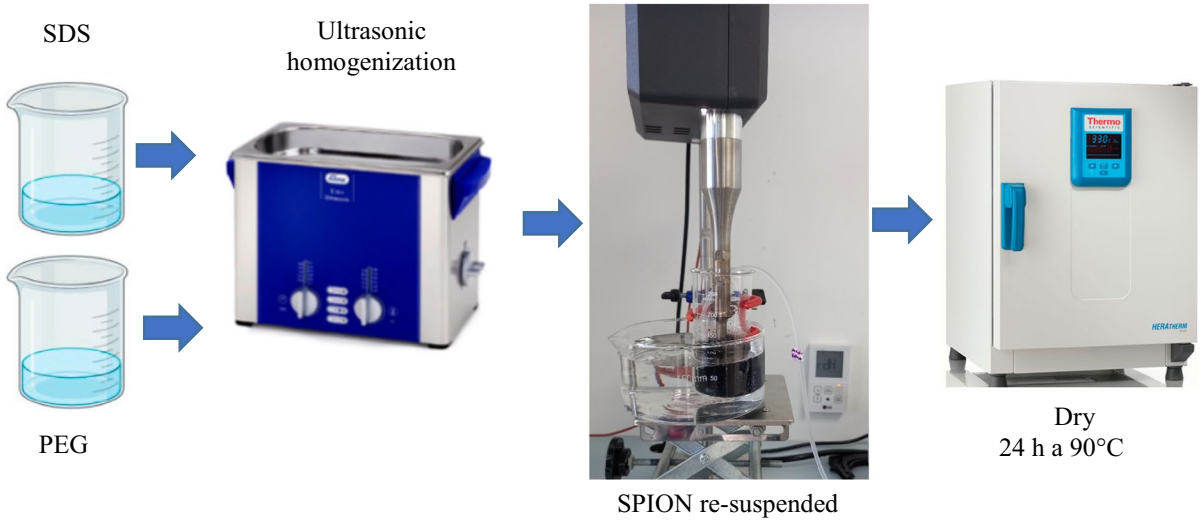


Fig. 3 SPION coating with PEG

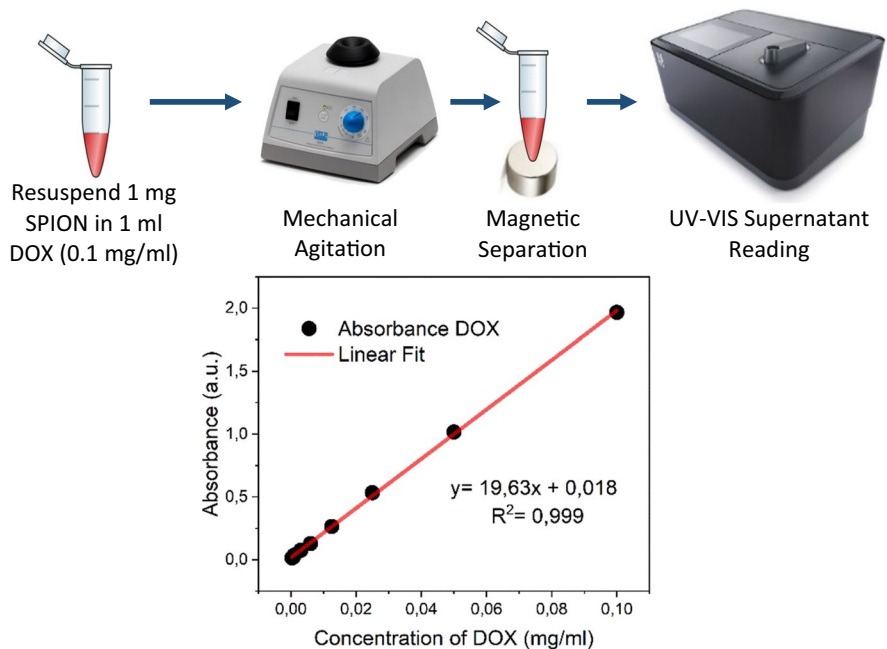
coated were dried in an oven for 24 h at 90 °C for characterization.

Doxorubicin adsorption: formation of the SPION@PEG@DOX system

The adsorption capacity of the SPION@PEG system was determined through the physisorption of

doxorubicin. As shown in Fig. 4, 1 mg of SPION@PEG was suspended in 1 mL DOX with a concentration of 0.1 mg/mL (according to the procedure described by Kuznetsov et al.) and kept in mechanical agitation at 1500 rpm for 60 min. After this time, the SPION@PEG was decanted using a permanent magnet, obtaining the nanocomposite SPION@PEG@DOX. Finally, the optical density of the supernatant

Fig. 4 DOX adsorption and DOX calibration curve



was measured with a UV–VIS spectrum of 300 to 650 nm (Merck, Spectroquant® Prove 600) to determine the concentration of DOX adsorbed by the SPION. The concentration of the adsorbed drug was calculated as the difference between the initial DOX concentration and the DOX concentration present in the supernatant. The DOX concentration in the supernatant was calculated based on the calibration curve presented in Fig. 4. The absorbance of a series of DOX solutions was measured to obtain this graph. From the calibration data points, the equation of the line was obtained, with a linear fit with a value of $R^2=0.999$.

Physicochemical characterization

The characterization was made for SPION, SPION@PEG and SPION@PEG@DOX. An X-ray diffractometer PANalytical model X'PERT PRO MPD with Cu-K α radiation ($\lambda=0.154056$ nm) was used to obtain the X-ray diffraction pattern. The program X-Pert High Score plus version 3.0 of Panalytical was used to identify the peaks and phases. The morphological characterization of the particles was performed using a TESCAN FE-MEB LYRA3 scanning electron microscope (SEM) operating at 30 kV and a Tecnai F20 Super Twin TMP transmission electron microscope (TEM) of FEI operating at 200 kV. Structural characterization of NPs was performed by high-resolution transmission electron microscopy (HRTEM) analysis and select-area electron diffraction pattern (SAED). The SEM and TEM teams have an integrated energy-dispersive X-ray spectrometry (EDS) microanalysis system, which allowed them to identify the chemical elements present in the samples and the relative percentage of each of them. The samples for SEM and TEM were prepared by dispersing the nanoparticles in water for 10 min by ultrasound. The suspension was then deposited on a carbon-backed copper TEM grid (Lacey carbon) to vacuum dry. Fourier transforms infrared spectrometry (FTIR) was used to confirm these results, which were recorded with a Bruker-Alpha spectrometer at a resolution of 4 cm $^{-1}$. FTIR spectra were measured between 400 and 4000 cm $^{-1}$.

The magnetic characterization of the samples was performed by vibrating sample magnetometry (VSM), which allowed obtaining the magnetic hysteresis curve using a Quantum Design magnetometer

(VersaLab TM) at 300 K, with an applied field of -30 kOe to 30 kOe. The DOX concentration was determined with a UV–VIS spectrophotometer (Merck, Spectroquant® Prove 600) equipped with 1-cm optical length cuvettes.

Cellular cytotoxicity by MTT assay

Before the laboratory process, the design of the plate of 96 wells was carried out. Twenty thousand cells were seeded in medium supplemented at 10%. Then, the dish was incubated at 37 °C for 24 h. After this time, the stimulus to be evaluated (SPION, SPION@PEG and SPION@PEG@DOX) was added according to the concentration designated in the corresponding wells (Table 1) and incubated for 48 h at 37 °C. Subsequently, 10 μ L of MTT reagent was added to each well, and the plate was placed for 4 h until the crystal formation was observed. Once this process was completed, the medium was removed, and 100 μ L of DMSO was added; the plate was left in the incubator for 20 min to dissolve the crystals. Finally, the board was read at 570 nm on the microplate reader (Corning® 96 Well CellBIND).

Statistical analysis

The distribution of NP sizes obtained by TEM images was made with the ImageJ software using a LogNormal setting, allowing us to get the average size and standard dispersion. The data obtained from the cell viability assay were analysed with GraphPad 8, and the level of significance in all statistical analyses was established as a probability of $p < 0.05$. Statistical significance was determined using two-way ANOVA. Data normality was checked with a Shapiro–Wilk test, and a paired test was performed with the t -student test to identify significant differences between groups.

Results and discussion

The structural, morphological, magnetic and chemical properties of SPION, SPION@PEG and SPION@PEG@DOX are presented below. DRX, SEM, TEM, EDS, FTIR and VSM techniques were employed to characterize the nanoparticles.

Table 1 Concentrations and treatments used in the MTT trial

	1	2	3	4	5	6	7	8	9	10	11	12
A	Cells			SPION-PEG 25 µg/ml*			DOX 0.0252 mg/ml			SPION-PEG 25 µg/ml		
B	Cells			SPION-PEG 50 µg/ml*			DOX 0.0126 mg/ml			SPION-PEG 50 µg/ml		
C	Mediums*			SPION-PEG 100 µg/ml*			DOX 0.0063 mg/ml			SPION-PEG 100 µg/ml		
D	Mediums *			SPION-PEG 200 µg/ml*			DOX 0.00315 mg/ml			SPION-PEG 200 µg/ml		
E	SPION 25 µg/ml*			SPION-PEG-DOX 25 µg/ml*			SPION 25 µg/ml			SPION-PEG-DOX 25 µg/ml		
F	SPION 50 µg/ml*			SPION-PEG-DOX 50 µg/ml*			SPION 50 µg/ml			SPION-PEG-DOX 50 µg/ml		
G	SPION 100 µg/ml*			SPION-PEG-DOX 100 µg/ml*			SPION 100 µg/ml			SPION-PEG-DOX 100 µg/ml		
H	SPION 200 µg/ml*			SPION-PEG-DOX 200 µg/ml*			SPION 200 µg/ml			SPION-PEG-DOX 200 µg/ml		

* Corresponds to white

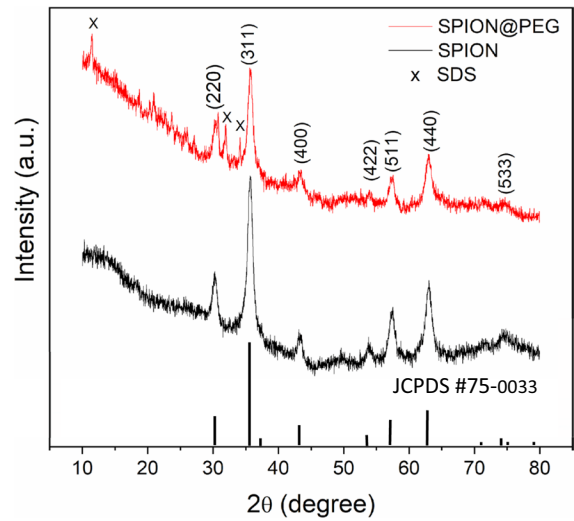


Fig. 5 XRD patterns of PEG-coated magnetite (red line), uncoated (black line) and Fe₃O₄ magnetite (JCPDS #75-0033)

Crystal structure: XRD and SAED

The X-ray diffraction patterns of the uncoated SPIONs and SPION@PEG are shown in Fig. 5. The 2θ values of 30.3°, 35.6°, 43.3°, 53.8°, 57.3° and 62.9° corresponding to the crystallographic planes (220), (311), (400), (422), (511) and (440), of the cubic crystal structure of inverse spinel space group *Fd3m*, this structure is typical of the magnetite Fe₃O₄. The positions of the peaks and their relative intensities of the XRD obtained were compared with the JCPDS crystallographic card #75-0033 of Fe₃O₄ magnetite [27, 28], confirming the phase obtained. It is observed that the peaks of the diffractogram have a considerable width, indicating the existence of particles with a grain on the nanometric scale. Using Scherrer's equation, $D = K\lambda/\beta \cos(\theta)$, where *D* is the size of the crystalline domains (crystal or crystallite size), λ is the wavelength of the X-rays, β is the average height width of the analysed peak, θ is the angle of reflection of the strongest signal, and *K* is the form factor, assuming spherical crystals takes a typical value of 0.9 [29], and using diffraction peak widening (311), the average diameter of the crystallites was determined. The sizes obtained were 9.86 nm without coating and 9.53 nm coated. The positions of the characteristic peaks of uncoated and PEG-coated SPIONs remain constant in the diffraction pattern, indicating that the coating does not change the crystal

structure of the Fe_3O_4 core. However, in the case of PEG-coated SPION, it can be observed that the height of the peaks decreases due to the amorphous coating of the PEG. The low-intensity signals indicated as (X) possibly correspond to forming a second crystalline phase related to SDS which corresponds to sodium sulfate (Na_2SO_4) with orthorhombic symmetry and space group $Pnna$ (52). Finally, no other peak associated with any different polluting phase was observed. The size found of the crystallite allows classifying the NPs synthesized in VSPIO since the superparamagnetic iron nanoparticles are classified according to their diameter, the SPIONS as the general group, less than 150 nm, ultra-small superparamagnetic iron oxide NPs (USPIO) less than 50 nm and very small iron oxide NPs (VSPIO) less than 10 nm [30].

Figure 6 corresponds to the selected area electron diffraction (SAED) pattern of the SPION and SPION@PEG samples, where the satisfactory

crystallinity of these NPs is revealed. The patterns exhibit different intensities of bright circular rings related to the planes (220), (311), (400), (422), (511) and (440) that are identified in the spinel structure of Fe_3O_4 [30], proving that the spinel-like structure of Fe_3O_4 does not change when coated with PEG. These results confirm the analysis performed on the XRD patterns in Fig. 6.

Figure 7 a shows the HRTEM image of the SPION core showing the interplanar distances $d_1=4.84 \text{ \AA}$, $d_2=2.96 \text{ \AA}$, $d_3=2.53 \text{ \AA}$, $d_4=2.11 \text{ \AA}$, which correspond to the planes (111), (220), (311) and (400) respectively. This can also be confirmed by the fast Fourier transform (FFT) pattern shown in Fig. 8(b), where the planes (111), (220), (311), (400), (511) and (422) corresponding to the magnetite phase are identified [31]. Figure 7(c) shows a model of Fe_3O_4 (magnetite) with inverse spinel structure and space group $Fd3m$. This corroborates the formation of a

Fig. 6 SAED: **a** SPION and **b** SPION@PEG

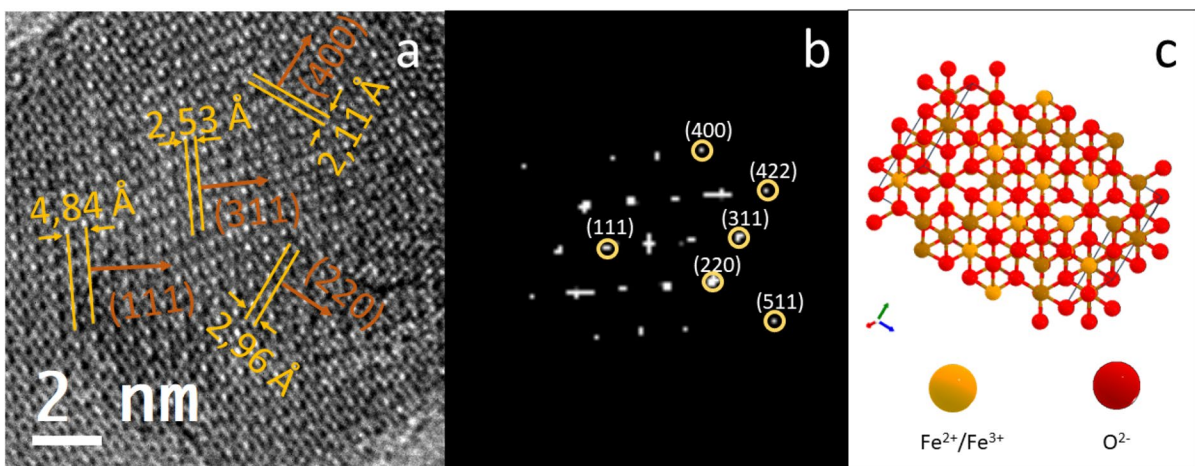
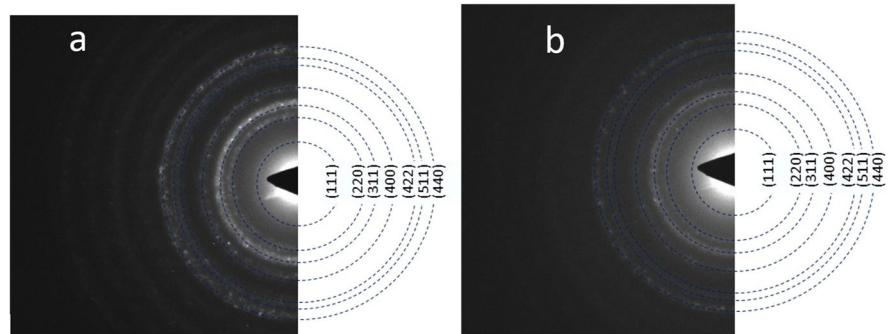


Fig. 7 **a** HRTEM of the SPION nucleus **b** FFT of **a** and **c** magnetite structure

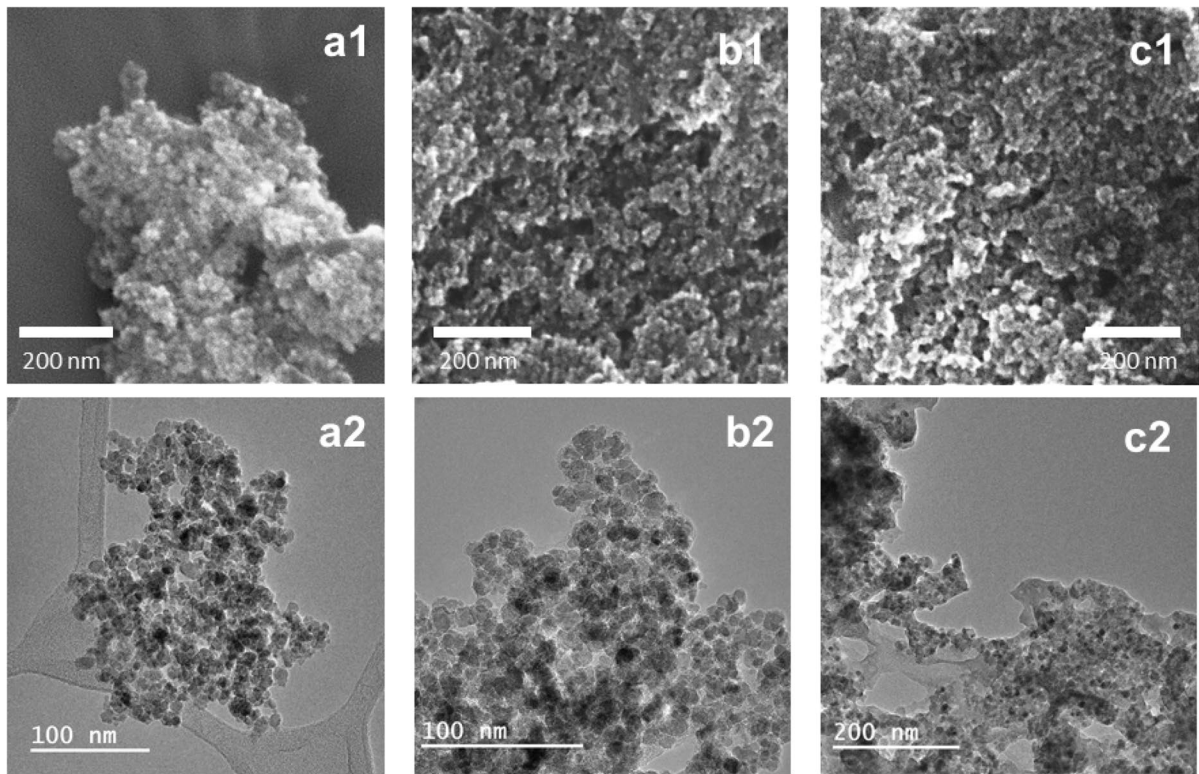


Fig. 8 SEM and TEM of (a) SPION, (b) SPION@PEG, and (c) SPION@PEG@DOX

single-crystalline phase in the nucleus of the NPs corresponding to magnetite.

Morphological characterization

The morphology and size of the SPION, SPION@PEG and SPION@PEG@DOX were determined by analysing images (Fig. 8) obtained by SEM (upper row) and TEM (lower row). Figure 9 a shows the uncoated SPION; the aggregation of the NPs is possibly a consequence of the preparation of the sample on the TEM grid. Figure 8 (b1 and b2) shows the SPION@PEG, and Fig. 9 c shows the SPION@PEG@DOX. Based on the micrographs observed, it can be established that the nanoparticles exhibit a spheroidal morphology; this morphological characteristic is of relevance in applications in biomedicine since the NPs with spherical shape can offer a uniform coating, which means that more drugs can be loaded on the surface of the nanoparticles for a better release of this at the target site and, therefore, they exhibit greater cellular toxicity [32]. Using the

ImageJ software, the size distribution was determined by measuring 100 NPs in the TEM micrographs; the adjustment was made by a monomodal LogNormal distribution, which represents the best adjustment curve to find the average diameter. In this way, it was determined that the nanoparticles had an average size of 9.37 ± 0.39 nm (SPION), 10.76 ± 0.61 nm (SPION@PEG) and 11.61 ± 0.89 nm (SPION@PEG@DOX) (Fig. 9).

The sizes found were consistent with the crystallite size (9.86 nm without coating and 9.53 nm with PEG coating), with which it can be inferred that the NPs have high crystallinity; this characteristic is crucial since it influences the magnetic properties [33]. In the SPION (Fig. 9a), the formation of any layer on its surface is not observed, confirming that the washing and drying processes were carried out properly since no layers of oxides or salts are formed from the precursors used. The increase in the diameter of the SPION@PEG compared to the SPION is due to the formation of the PEG layer that covers them. This layer has an average thickness of 1.39 nm (although

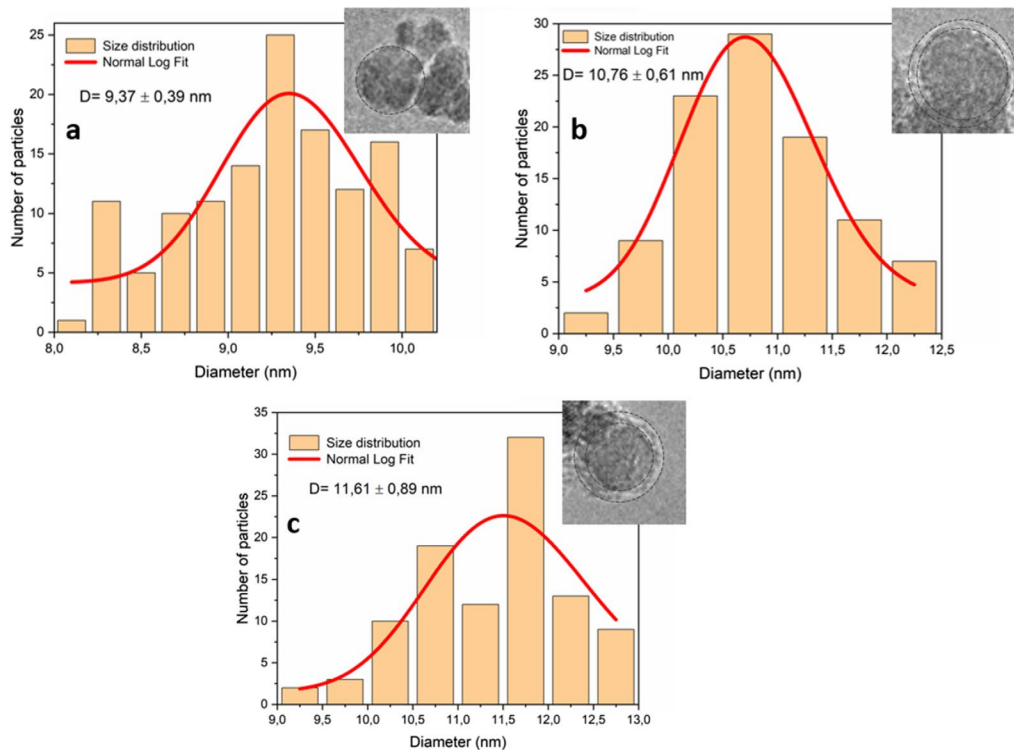


Fig. 9 Size distribution for **a** SPION, **b** SPION@PEG, and **c** SPION@PEG@DOX

the coating is not uniform if it covers the entire nanoparticle). In the same way, the increase in the diameter of the SPION@PEG@DOX is due to the adhesion of the DOX to the particles SPION@PEG, forming a second layer with an average thickness of 0.85 nm.

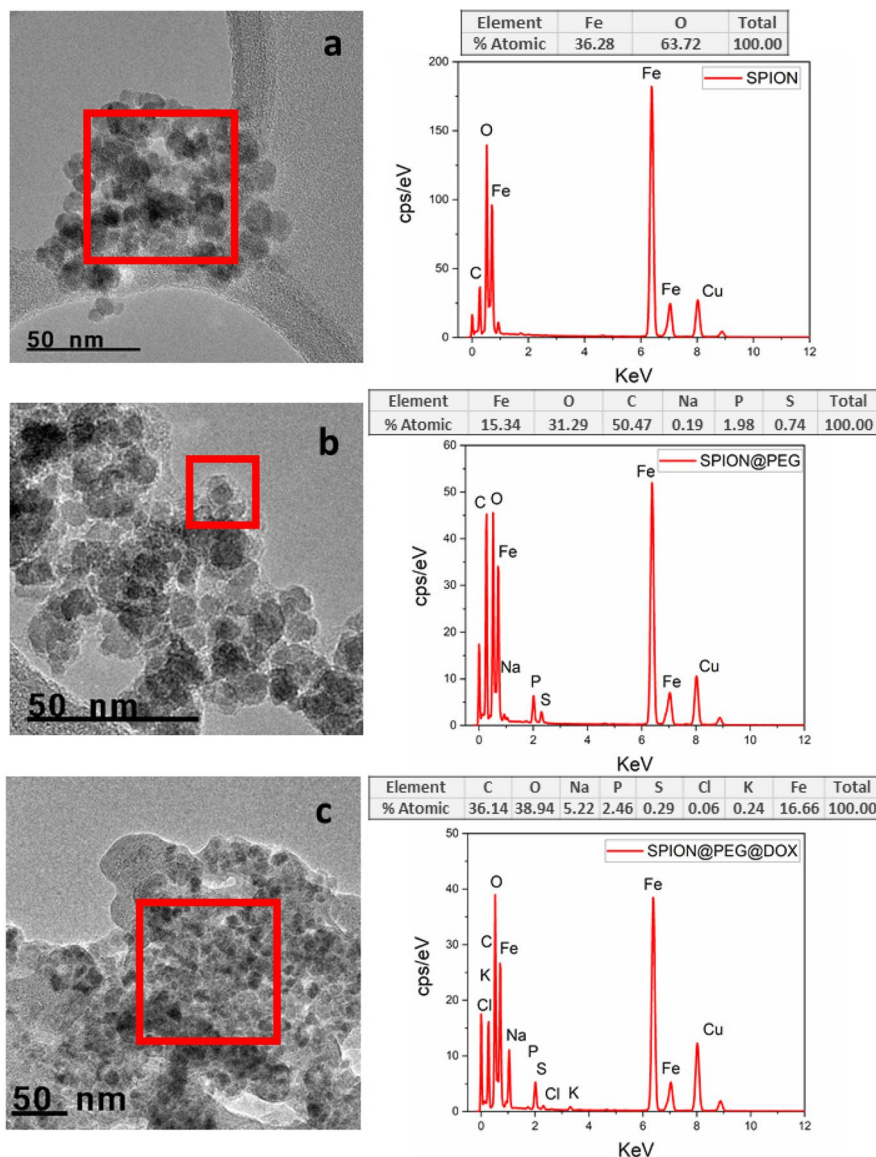
As the size of these NPs is essential in the adhesion and interaction with the cells of the organism, the diameter of the NPs obtained in this work makes them excellent candidates for applications in medicine. For example, for oral administration of anticancer drugs, the possible mechanisms in which nanoparticles can cross gastrointestinal barriers are paracellular passage (<50 nm), endocytic uptake (<500 nm) and lymphatic uptake (<5 μ m) [35]. Another example is the intravenous administration of anticancer drugs, where the morphology of NPs determines their pharmacokinetic behaviour since the elimination of NPs in the blood system is due to the reticuloendothelial system (MPS). This system consists of bone marrow progenitor cells, blood monocytes and tissue macrophages, such as Kupffer cells, to recognize and eliminate microorganisms, senescent cells and other external elements [36]. MPS recognizes the NPs and

is eliminated from the blood system, decreasing the chance of being bioaccumulated at the target site. NPs with a diameter greater than 200 nm are phagocytosed and bioaccumulated in the spleen. In comparison, NPs with a diameter of less than 40 nm and additional with a hydrophilic coating, such as PEG, have a plasma half-life of over 2 h [36].

Chemical characterization: EDS and FTIR

Figure 10 shows the X-ray energy scattering spectroscopy (EDS) spectra and their respective semi-quantitative elemental analysis. In the TEM micrographs, the areas analysed are shown in red. The spectrum of uncoated SPION (Fig. 11a) shows that iron and oxygen have an atomic percentage of 36.28% and 63.72%, respectively, confirming a successful elemental composition of the nucleus of the NPs. The spectrum obtained from SPION@PEG (Fig. 10b) confirms that the core mainly comprises iron and oxygen. Sodium and sulfur come from the SDS used in the synthesis during functionalization with PEG. Although clearly in the TEM micrograph, the formation of a layer that

Fig. 10 EDS of **a** SPION, **b** SPION@PEG, and **c** SPION@PEG@DOX. The red boxes show the area analysed by EDS



covers the nucleus of the NPs is observed (Fig. 10a), it is not possible to confirm by EDS that its composition is PEG since it is composed of carbon like the support of the grid used for TEM (Lacey carbon). However, a significant increase in the carbon signal compared to the EDS of the SPION suggests that this coating is composed of PEG. The spectrum of the SPION@PEG@DOX (Fig. 11c) also shows chlorine (0.06%), evidencing the presence of DOX by the hydrochlorides in the DOX used, confirming the functionalization of the NPs with the drug. The copper seen in all samples comes from the TEM (Lacey

carbon) grid. These results prove that the methodology for forming the nanocomposite is adequate, minimizing external pollutants.

FTIR was used to corroborate the functionalization of SPION with PEG and DOX. Figure 11 illustrates the FTIR spectra of SPION, SPION@PEG, PEG and SPION@PEG@DOX. The band displayed on 580 cm^{-1} is characteristic of the stretching vibrations of the Fe–O bond in the crystal lattice Fe_3O_4 , which also confirms the magnetite core in all samples. Its surface is covered with hydroxyl groups whenever the synthesis is advanced in an aqueous medium.

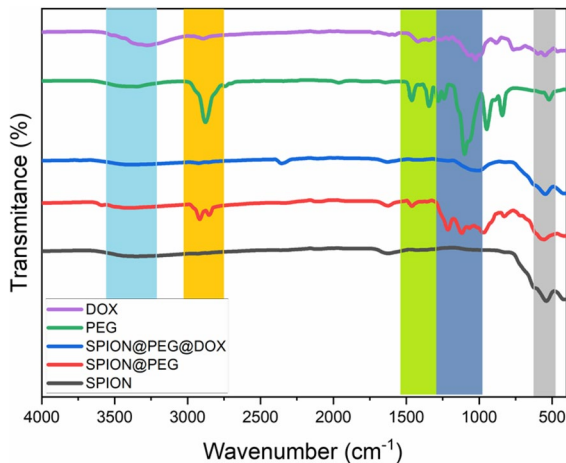
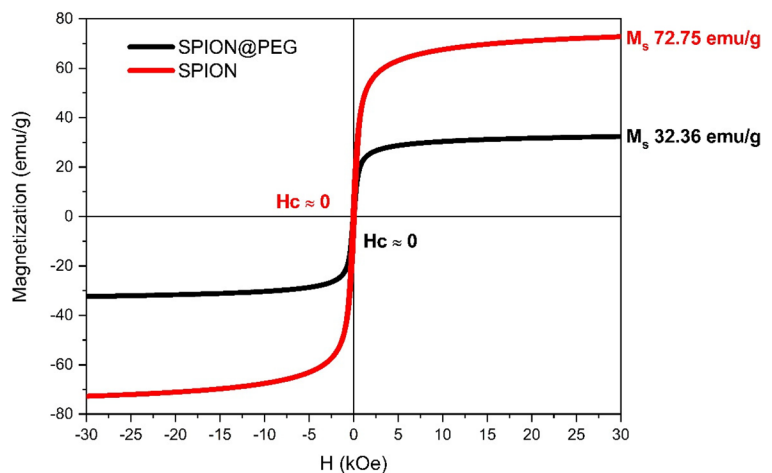


Fig. 11 FTIR. Characteristic bands of stretching and bending vibrations for SPION, SPION@PEG, and SPION@PEG@DOX

The characteristic bands are observed in 1.636 and 3.415 cm^{-1} , corresponding to the bending vibration of H–O–H in the samples [37, 38].

The appearance and increase in the stretching band C–H to 2,915 cm^{-1} and the bending band C–H₂ and C–H₃ to 1,636 cm^{-1} were observed, confirming the formation of the PEG layer (SPION@PEG). The bands close to 1200 cm^{-1} belong to the C–O–C stretching vibration of the repeated units –O–CH₂–CH₂– of polyethylene glycol [39]. The characteristic bands of DOX appeared in 2900, 1600 and 1027 cm^{-1} [40, 41], which confirms the functionalization of NPs with the drug; however, the characteristic bands of DOX have a shielding by the PEG since the distinctive bands are

Fig. 12 Magnetic hysteresis curve using uncoated SPION VSM and SPION@PEG



very similar. It can be observed how the typical signal of iron in 580 cm^{-1} is shielded as the PEG and DOX layers are formed on the core of the NPs, generating a less pronounced signal.

Magnetic properties

Figure 12 shows the magnetic hysteresis loops of the SPION and SPION@PEG at 300 K. Magnetization data was recorded while the applied field varied between –30 and 30 kOe. The graph shows that both samples present a superparamagnetic behaviour with zero remanences and coercivity. The saturation magnetization (M_s) values are 72.75 emu/g for uncoated SPIONs and 32.36 emu/g for SPION@PEG. It is observed that the SPION@PEG has a lower saturation magnetization than the uncoated SPION, probably due to the dilution of magnetic material within the volume of the sample when it is coated with the non-magnetic material, i.e. the moment per unit volume (and hence the moment per unit mass) is reduced [8]. However, it may also depend on the thickness of the silica layer; the thicker the SPION@PEG layer, the lower the saturation magnetization [42]. The coercive field (H_c) is approximately equal to zero, indicating that the dipoles are oriented randomly without a magnetic field, making the resulting magnetic moment zero. The lack of magnetic remanence is essential in medical applications. When NPs are subjected to a magnetic field, they are allowed to be guided to an objective point, and when this magnetic field has been eliminated, the redispersion of these NPs will take place quickly [43]. Additionally, it is an important

property when used in a biological system because if these NPs presented a magnetic remanence (ferromagnetic behaviour), dipole–dipole magnetic attractions would be generated between them, and they will agglomerate and form agglomerations, increasing the virtual size of NPs [44].

Superparamagnetic behaviour in NPs is related to size, shape and crystal structure. The high saturation magnetization and its superparamagnetic behaviour obtained in the NPs of SPION@PEG is a product of its high crystallinity, and low anisotropy confirmed in XRD and HRTEM, in addition to its nanometric size of less than 20 nm, was demonstrated through the different characterization techniques used. All this makes these NPs excellent candidates for applications in nanomedicine [12, 33, 45].

Cellular cytotoxicity by MTT assay

Figure 13 shows the percentage of metabolic activity evaluated by MTT (cell viability) after 48 h of exposure of Hela cells with SPION, SPION@PEG and SPION@PEG@DOX with different concentrations of doxorubicin (DOX) adsorbed. It is observed that exposure of Hela cells to the highest concentration of NPs (200 µg/ml) for 48 h generates an average cell viability of 55.5% with SPION, 76.7% with SPION@PEG and 45.5% with SPION@PEG@DOX (25 µg/mL DOX). While in the lowest concentration of NPs (25 µg/ml), a cell viability of 76.9% is observed with

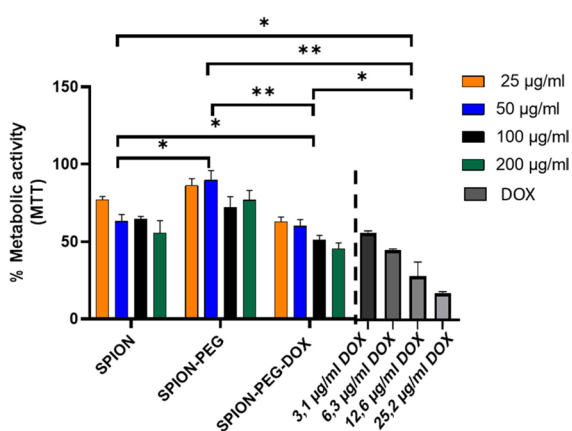


Fig. 13 Metabolic activity (cell viability) of Hela cells with different NPs (SPION, SPION@PEG and SPION@PEG@DOX) at different concentrations after 48 h of exposure. * p -value < 0.05; ** p -value < 0.01

SPION, 86.1% with SPION@PEG and 62.5% with SPION@PEG@DOX (3.1 µg/mL DOX). SPIONs coated with PEG have greater cell viability, showing that PEG anchored to NPs is an excellent platform to reduce damage to cells generated by uncoated NPs (SPION), which agrees with what has been reported by [13], and allows the adsorption of doxorubicin. This is evidenced by the effect generated by SPION@PEG@DOX on Hela cells.

To determine if there are significant differences in cell viability after exposure to each of the NPs at different concentrations, statistical analyses were performed using the ANOVA and t -student tests. First, we analysed whether the data showed normal behaviour with the Shapiro–Wilk test. Data from all groups showed a normal distribution ($p < 0.05$).

Differences between treatments (SPION, SPION@PEG, SPION@PEG@DOX) and nanoparticle concentrations (25, 50, 100 and 200 µg/ml) were analysed using the two-way ANOVA test. A significant difference in cell viability was found between treatments (p -value < 0.0001) and concentrations (p -value < 0.0001). A paired test was performed using the t -student test to identify which treatment groups had significant differences in cell viability. It was found that if there are substantial differences (p -value < 0.05) in the viability of the cells when they are treated with each of the NPs: SPION vs SPION@PEG (p -value: 0.0406); SPION vs SPION-PEG-DOX (p -value: 0.0271); SPION-PEG vs. SPION@PEG@DOX (p -value: 0.0018); DOX vs. SPION (p -value: 0.0140); DOX vs. SPION@PEG (p -value: 0.0056) and SPION@PEG@DOX (p -value: 0.0375).

Likewise, significant differences in cell viability were found in all groups of NPs in the following concentrations: 25 µg/mL vs. 100 µg/mL (p -value: 0.0251); 25 µg/mL vs. 200 µg/mL (p -value: 0.0417); 50 µg/mL vs. 200 µg/mL (p -value: 0.0388). At the following concentration, no significant differences in cell viability were found: 25 µg/mL vs. 50 µg/mL (p -value: 0.2190); 50 µg/mL vs. 100 µg/mL (p -value: 0.1039) and 100 µg/mL vs. 200 µg/mL (p -value: 0.2319).

The antitumoural effect of the nanocomposite SPION@PEG@DOX depends on the concentration. When the concentration was 200 µg/mL, the viability was less than 50%, while with the lowest concentrations, the viability was greater than 50%. The trial also showed that SPION@PEG@DOX

could maintain the integrity and activity of DOX by making it a good nanocomposite for the delivery of anticancer drugs.

Conclusions

The crystal structure of the synthesized iron oxide nanoparticles corresponds to the magnetite reverse spinel. This structure is associated with an “ultra-small” core of Fe_3O_4 , which remains unchanged even after coating it with polyethylene glycol or functionalizing this compound with doxorubicin.

The SPION, SPION@PEG and SPION@PEG@DOX have spheroidal morphology and an average diameter of 9.37, 10.76 and 11.61 nm, respectively. The increase in diameter is due to the coating by PEG (with a thickness of 1.39 nm) and functionalizing it with the DOX (a thickness of 0.85 nm).

The chemical composition of the synthesized nanocomposite confirms the presence of PEG and DOX. When analysing the vibration bands in FTIR, the interaction in the nanocomposites Fe_3O_4 @PEG and Fe_3O_4 @PEG@DOX is evident when observing the characteristic peaks corresponding to the vibrations of stretching or bending of the bonds present in each step of the synthesis.

SPION and SPION@PEG exhibit superparamagnetic behaviour, although PEG coating shows shielding, and the sample still has significant saturation magnetization.

The MTT assay confirmed a cell viability of less than 50% using the highest concentration (200 $\mu\text{g}/\text{mL}$) of the nanocomposite Fe_3O_4 @PEG@DOX, maintaining the integrity and activity of the DOX.

The nanocomposite Fe_3O_4 @PEG@DOX synthesized, considering the physicochemical characteristics identified, has the potential to be applied in developing cancer treatments.

Funding Open Access funding provided by Colombia Consortium. The authors received financial support from MINCIENCIAS [project code CT-672–2018 (Code 123377757091)] and Universidad Antonio Nariño [project code 2019227] as the technical support of the Nanomaterials lab.

Declarations

Conflict of interest The authors declare no competing interests.

Open Access This article is licensed under a Creative Commons Attribution 4.0 International License, which permits use, sharing, adaptation, distribution and reproduction in any medium or format, as long as you give appropriate credit to the original author(s) and the source, provide a link to the Creative Commons licence, and indicate if changes were made. The images or other third party material in this article are included in the article’s Creative Commons licence, unless indicated otherwise in a credit line to the material. If material is not included in the article’s Creative Commons licence and your intended use is not permitted by statutory regulation or exceeds the permitted use, you will need to obtain permission directly from the copyright holder. To view a copy of this licence, visit <http://creativecommons.org/licenses/by/4.0/>.

References

1. León MFC et al (2023) Cáncer de Cérvix y virus del papiloma humano. Diagnóstico y prevención. *Medicinas UTA* 7(2):2–8
2. National Cancer Institute (2019) Types of Cancer Treatment. National Institutes of Health. <https://www.cancer.gov/about-cancer/treatment/types>. Accessed 1 Nov 2023
3. Poole CP, Owens FJ (2007) Introducción a la nanotecnología. Reverté, España
4. Oropeza-Núñez RM, Jáuregui-Haza JU (2012) Nanoparticles as drug-deliverers: characteristics and perspectives. *Revista CENIC Ciencias Biológicas* 43:Sep.-Dic
5. Parveen S, Sahoo SK (2006) Nanomedicine: clinical applications of polyethylene glycol conjugated proteins and drugs. *Clin Pharmacokinet* 45:965–988
6. McNeil SE (2005) Nanotechnology for the biologist. *J Leukoc Biol* 78(3):585–594
7. Foldvari M, Bagonluri M (2008) Carbon nanotubes as functional excipients for nanomedicines: II. Drug delivery and biocompatibility issues. *Nanomedicine: Nanotechnol Biol Med* 4(3):183–200
8. Patil-Sen Y et al (2020) Biocompatible superparamagnetic core-shell nanoparticles for potential use in hyperthermia-enabled drug release and as an enhanced contrast agent. *Nanotechnology* 31(37):375102
9. Mohammadi MA, Asghari S, Aslibeiki B (2021) Surface modified Fe_3O_4 nanoparticles: a cross-linked polyethylene glycol coating using plasma treatment. *Surf Interfaces* 25:101271
10. Munnier E, Cohen-Jonathan S, Linassier C, Douziech-Eyrolles L, Marchais H, Soucé M, Chourpa I (2008) Novel method of doxorubicin–SPION reversible association for magnetic drug targeting. *Int J Pharm* 363(1–2):170–176
11. Guivar JR, Domínguez AB, Carbajal LM, Osorio AM, De Los Santos L, Barne CHW (2013) Nanopartículas de óxido de hierro superparamagnéticas (SPIONS): Propiedades estructurales y magnéticas para posibles aplicaciones biomédicas. *Rev Investig Fís* 16(02):1–5
12. Dulińska-Litewka J, Łazarczyk A, Hałubiec P, Szafranski O, Karnas K, Karewicz A (2019) Superparamagnetic iron oxide nanoparticles—current and prospective medical applications. *Materials* 12(4):617

13. Santa CF, López Osorio BL (2013) Materiales poliméricos en nanomedicina: transporte y liberación controlada de fármacos. *Rev Acad Colomb Cienc Exactas Fisic Nat* 37(142):115–124
14. Knop K, Hoogenboom R, Fischer D, Schubert US (2010) Poly (ethylene glycol) in drug delivery: pros and cons as well as potential alternatives. *Angew Chem Int Ed* 49(36):6288–6308
15. Urrejola MC, Soto LV, Zumarán CC, Peñaloza JP, Álvarez B, Fuentesvilla I, Haidar ZS (2018) Sistemas de nanopartículas poliméricas II: estructura, métodos de elaboración, características, propiedades, biofuncionalización y tecnologías de auto-ensamblaje capa por capa (layer-by-layer self-assembly). *Int J Morphol* 36(4):1463–1471
16. Esquivel-Figueroa RDLC, Mas-Diego SM (2021) Síntesis biológica de nanopartículas de plata: revisión del uso potencial de la especie *Trichoderma*. *Rev Cuba Química* 33(2):23–45
17. Someya S, Yoshiki Y, Okubo K (2002) Antioxidant compounds from bananas (*Musa Cavendish*). *Food Chem* 79(3):351–354
18. González-Montelongo R, Lobo MG, González M (2010) Antioxidant activity in banana peel extracts: testing extraction conditions and related bioactive compounds. *Food Chem* 119(3):1030–1039
19. Torres-Arellano S et al (2021) Biosynthesis of cuprous oxide using banana pulp waste extract as a reducing agent. *Fuel* 285:119152
20. Halevas EG, Pantazaki AA (2018) Copper nanoparticles as therapeutic anticancer agents. *Nanomed Nanotechnol J* 2(1):119–139
21. Alvarado Meza R (2014) Síntesis sonoquímica de nanopartículas de óxido de cinc y de plata estabilizadas con quitosano. Evaluación de su actividad antimicrobiana. *Revista Iberoamericana de Polímeros* 15(2):134–148
22. Yousefi S, Ghasemi B, Nikolova MP (2021) Opto-structural characterization of Mg(OH)₂ and MgO nanostructures synthesized through a template-free sonochemical method. *Appl Phys A* 127(7):549
23. Changlin YU et al (2012) Sonochemical fabrication of novel square-shaped F doped TiO₂ nanocrystals with enhanced performance in photocatalytic degradation of phenol. *J Hazard Mater* 237:38–45
24. Shin N, Saravanakumar K, Wang MH (2019) Sonochemical mediated synthesis of iron oxide (Fe₃O₄ and Fe₂O₃) nanoparticles and their characterization, cytotoxicity and antibacterial properties. *J Cluster Sci* 30:669–675
25. Petigny L et al (2013) Batch and continuous ultrasound-assisted extraction of boldo leaves (*Peumus boldus* Mol.). *Int J Mol Sci* 14(3):5750–5764
26. Alfaro JAA (2010) Síntesis y deposición sonoquímica de nanopartículas de plata sobre placas de ABS y evaluación de su actividad antimicrobiana. Tesis, Centro de investigación en química aplicada
27. Wang YM et al (2011) Synthesis of Fe₃O₄ magnetic fluid used for magnetic resonance imaging and hyperthermia. *J Magn Magn Mater* 323(23):2953–2959
28. Chen C et al (2022) Recyclable and high-efficiency methane hydrate formation promoter based on SDS-coated superparamagnetic nano-Fe₃O₄. *Chem Eng J* 437:135365
29. Abdullah M, Khairurrijal K (2009) Derivation of Scherrer relation using an approach in basic physics course. *Jurnal Nanosains Nanoteknologi* 1(1):28–32
30. Shan L (2010) Superparamagnetic iron oxide nanoparticles (SPION) stabilized by alginate. *Molecular Imaging and Contrast Agent Database (MICAD)* 2004–2013
31. Yu J et al (2022) Fabrication of Fe₃O₄ nanoparticles by using cathode glow discharge electrolysis plasma and its electrochemical properties. *Electrochim Acta* 427:140843
32. Martínez-Mera I, Espinosa-Pesqueira ME, Pérez-Hernández (2007) Synthesis of magnetite (Fe₃O₄) nanoparticles without surfactants at room temperature. *Mater Lett* 61(23–24):4447–4451
33. Yew YP et al (2020) Green biosynthesis of superparamagnetic magnetite Fe₃O₄ nanoparticles and biomedical applications in targeted anticancer drug delivery system: a review. *Arab J Chem* 13(1):2287–2308
34. Qing I et al (2017) Correlation between particle size/domain structure and magnetic properties of highly crystalline Fe₃O₄ nanoparticles. *Sci Rep* 7(1):9894
35. Win KY, Feng S-S (2005) Effects of particle size and surface coating on cellular uptake of polymeric nanoparticles for oral delivery of anticancer drugs. *Biomaterials* 26(15):2713–2722
36. Hilger I, Kaiser WA (2012) Iron oxide-based nanostructures for MRI and magnetic hyperthermia. *Nanomedicine* 7(9):1443–1459
37. Yang K et al (2010) Re-examination of characteristic FTIR spectrum of secondary layer in bilayer oleic acid-coated Fe₃O₄ nanoparticles. *Appl Surf Sci* 256(10):3093–3097
38. Lopez JA et al (2010) Synthesis and characterization of Fe₃O₄ magnetic nanofluid. *Rev Latinoam Metal Mater* 30(1):60–66
39. Junejo Y, Baykal A, Sözeri H (2013) Simple hydrothermal synthesis of Fe₃O₄-PEG nanocomposite. *Open Chem* 11(9):1527–1532
40. Unsoy G et al (2014) Synthesis of doxorubicin loaded magnetic chitosan nanoparticles for pH-responsive targeted drug delivery. *Eur J Pharm Sci* 62:243–250
41. Karimi S, Namazi H (2021) Fe₃O₄@PEG-coated dendrimer modified graphene oxide nanocomposite as a pH-sensitive drug carrier for targeted delivery of doxorubicin. *J Alloy Compd* 879:160426
42. Morales F et al (2019) Structural and magnetic properties of silica-coated magnetite nanoaggregates. *Phys B: Condens Matter* 572:214–219
43. Chen X et al (2012) Novel superparamagnetic iron oxide nanoparticles for tumour embolization application: preparation, characterization and double targeting. *Int J Pharm* 426(1–2):248–255
44. Gupta AK, Gupta M (2005) Synthesis and surface engineering of iron oxide nanoparticles for biomedical applications. *Biomaterials* 26(18):3995–4021
45. Ghazanfari MR et al (2016) Perspective of Fe₃O₄ nanoparticles role in biomedical applications. *Biochem Res Int* 2016002E

Publisher's Note Springer Nature remains neutral with regard to jurisdictional claims in published maps and institutional affiliations.